Toward an Understanding of Intermediate- and Short-Range Defects in ZnO Single Crystals. A Combined Experimental and Theoretical Study†

R. C. Lima,‡ L. R. Macario,§ J. W. M. Espinosa,‡ V. M. Longo,§ R. Erlo,§ N. L. Marana,|| J. R. Sambrano,|| M. L. dos Santos,‡ A. P. Moura,§ P. S. Pizani,⊥ J. Andrés,§,# E. Longo,*,‡ and J. A. Varela‡

Instituto de Química, Universidade Estadual Paulista, Laboratório Interdisciplinar de Eletroquímica e Cerâmica, P.O. Box 355, 14800-900, Araraquara, SP, Brazil, Departamento de Química, Universidade Federal de São Carlos, Laboratório Interdisciplinar de Eletroquímica e Cerâmica, P.O.Box 676, 13565-905, São Carlos, SP, Brazil, Grupo de Modelagem e Simulação Molecular DM, Universidade Estadual Paulista, P.O.Box 473, 17033-360 Bauru, SP, Brazil, and Departamento de Física, Universidade Federal de São Carlos, P.O.Box 676, 13565-905, São Carlos, SP, Brazil

Received: March 14, 2008; Revised Manuscript Received: April 25, 2008

A joint use of experimental and theoretical techniques allows us to understand the key role of intermediate- and short-range defects in the structural and electronic properties of ZnO single crystals obtained by means of both conventional hydrothermal and microwave-hydrothermal synthesis methods. X-ray diffraction, Raman spectra, photoluminescence, scanning electronic and transmission electron microscopies were used to characterize the thermal properties, crystalline and optical features of the obtained nano and microwires ZnO structures. In addition, these properties were further investigated by means of two periodic models, crystalline and disordered ZnO wurtzite structure, and first principles calculations based on density functional theory at the B3LYP level. The theoretical results indicate that the key factor controlling the electronic behavior can be associated with a symmetry breaking process, creating localized electronic levels above the valence band.

Introduction

ZnO is a well recognized semiconducting and piezoelectric material. Their wide and tunable direct band gap energy of 3.37 eV with a large excitation binding energy of 60 meV at room temperature,[1] much larger than those of other semiconductor materials, means that this material finds a variety of uses in electronic industry such as photocatalysts, UV light-emitting diodes, laser diodes, solar cells, microsensors, and other devices.[2,3] ZnO has been attracting a lot of attention because of their unique properties and potential application, opening a surge in research activities from a practical and scientific point of view, including many interesting nanostructures such as belts, helices.[4,5] In addition, a plethora of ZnO morphologies have been synthesized and characterized in detail, such as nanoparticle,[6] nanorods,[7] nanowires,[8] nanotubes,[9] nanoflowers,[10] tetrapod,[11] doughnuts,[12] nanodisks, nanoplates, nanospheres and hemispheres.[13–19]

Vayssieres[20] reported that ZnO could easily be processed as nanowires or arrayed nanorods on solid supports by monitoring the hydrolysis of $Zn(NO_3)_2$. Zhang et al. have demonstrated that well-aligned ZnO nanowires were synthesized by simple physical vapor deposition using *c*-oriented ZnO thin films as substrates without catalysts or additives.[21,22] Gao and Wang have developed a Sn-catalyzed ZnO structure vapor−liquid−solid growth on a single-crystal ZnO substrate[22] and these authors explain how these nanoarchitectures grow by combining some of the fundamental structural configurations of ZnO.[23] In addition, Hughes and Wang[24] have proposed a theoretical model supporting the experimental data on the structural features of nanorings and nanobows formed by bending single-crystal of polar surface dominated ZnO nanobelts. Han et al.,[25] by using a simple low-temperature liquid-phase method, obtained large-scale arrays of highly oriented ZnO nanorods on ZnO-film-coated substrates of any class. Choi et al. have prepared ZnO nanoblade and nanoflower using zinc acetate dehydrate aqueous solution by ultrasonic pyrolisis.[26]

In recent years, many techniques and methods have been investigated for the obtention of ZnO nanostructures, such as thermal evaporation,[27–30] physical and chemical vapor deposition,[31–37] metal organic vapor-phase epitaxy,[38] microwave plasma desposition,[39] pyrolysis,[40] chemical bath deposition,[41,42] heterogeneous nucleation in mixed or/and aqueous solution,[43–46] and the hydrothermal method.[47–50] The hydrothermal method is a promising one for fabricating ideal nanomaterial with appropriate morphology and it is generally a low-temperature, low-cost process, high yield, scalable process for large fabrication of ZnO nanostructures. Different authors have demonstrated that hydrothermal conditions[51–55] can be used to successfully grown ZnO single crystals. Particles with a controllable size and shape, highly crystalline and low agglomeration can be obtained using this synthetic route. In addition, a variation of this technique, i.e., hydrothermal synthesis using microwave (microwave-hydrothermal), accelerates the crystallization process, increasing the nucleation rate and, hence, leads to the formation of fine particles with homogeneous distribution.[56,57] Freeman et al. have discussed the implications for the crystal growth of wurtzite materials, such as ZnO, based on periodic density functional calculations on ultrathin films,[58] and Terrones et at.[59] have

† Part of the special section for the "Symposium on Energetics and Dynamics of Molecules, Solids and Surfaces".

* Corresponding author. E-mail: elson@iq.unesp.br.
‡ Instituto de Química, Universidade Estadual Paulista.
§ Departamento de Química, Universidade Federal de São Carlos.
|| Grupo de Modelagem e Simulação Molecular DM, Universidade Estadual Paulista.
⊥ Departamento de Física, Universidade Federal de São Carlos.
On leave from Departamento de Química Física y Analítica, Universitat Jaume I, 12071 Castello, Spain.

10.1021/jp8022474 CCC: $40.75
Published on Web 07/25/2008

carried out first principles calculations on ZnO nanoribbons for zigzag and armchair terminated edges.

At room temperature the thermodynamically stable phase of ZnO is the hexagonal wurtzite crystal structure ($P6_3mc$) where each anion is surrounded by four cations at the corners of the tetrahedron. The unit cell has two atoms containing two units of ZnO. There are two nonequivalent atoms in the unit cell with internal experimental values: Zn ($^2/_3$, $^1/_3$, 0), O ($^2/_3$, $^1/_3$, μ), where μ is the internal parameter of wurtzite structure. Structurally, ZnO has a noncentral symmetric wurtzite crystal structure with a hexagonal Bravais lattice ($a = 3.250$ Å and $c = 5.207$ Å) and it can be depicted as alternanting planes of tetrahedrally coordinated O^{2-} and Zn^{2+} ions, stacked alternatively along the c-axis. This arrangement generates a dipole moment and a spontaneous polarization along this c-axis between the oppositely charged ions, i.e., positively charged Zn-(0001) and negatively charged O-(0001) polar surfaces.

For the sake of lacking the central symmetry in wurtzite, ZnO presents strong piezoelectric and pyroelectric properties and is ideally suitable for optical applications. Green (520 nm) and orange (620 nm) emission bands have been reported in both nanocrystals and bulk crystals, and they are associated with different defects produced during the synthesis process and are found to influenced by several factors, such as reaction temperature and presence of oxygen.[60] ZnO is transparent to visible light and can be made highly conductive by doping; in this context, the green emission band of ZnO has been studied by many groups and was assigned to the tunneling recombination of donor−acceptor (D−A) pairs.[3,61–65] As to the identity of the defect, it has been suggested to be copper impurities,[66] oxygen vacancies,[61,67] zinc interstitials,[68] and ZnO antisites.[69] Recent studies suggest a recombination of electrons from the conduction band or a level close to the conduction band edge with a deeply trapped hole in a $V_O^{\bullet\bullet}$ center to be the origin of the green emission.[3] First principle theoretical results by Zhang et al.[70] showed that oxygen vacancies have a low formation enthalpy and are easily formed. EPR results for the ZnO nanocrystals have manifested that the $V_O^{\bullet}$ centers are the predominant defects.[61,71] Furthermore, the nanowires with large surface-to-volume ratios have a lot of dangling bonds and defects on the surface, which can absorb the O^{2-} and O^- ions to form the O^{2-}/O^- surface system. Schoenmakers et al.[72] have demonstrated that this O^{2-}/O^- surface system is the predominant trapper of the holes in the valence band, which play a key role in the formation of the visible emission centers ($V_O^{\bullet\bullet}$).

The photoluminescent emission of semiconductors is an important material property because it can provide information on defects and relaxation pathways of excited states, depending upon the preparation techniques, which can generate different structural defects. Different photoluminescence experiments on ZnO-based systems have been performed and possible explanations have been proposed.[60,63,64,73] In this paper, the intermediate- and short-range defects in ZnO crystals using X-ray diffraction (XRD), Raman, and photoluminescence (PL) techniques are reported and different responses in the photoluminescent emission were also investigated. The two synthesis methods used in the ZnO powders preparation, conventional hydrothermal and microwave-hydrothermal, suggest different defects formation, which can be an indicative of different conformations into the hexagonal structure (wurtzite) during the ZnO growth.

We have been interested in the property of shape-controlled crystals, aiming to explore the PL properties of different crystals in terms of order−disorder. The research involves three critical steps: synthesis of shape-controlled crystals, structural characterization, and PL emission investigation. We also investigated the electronic structure using first-principles calculations based on the density functional theory (DFT). The purpose is to join both the experimental and theoretical results to explain the different responses of PL emission at room temperature of ZnO powders by using two different structural order−disorder, associated with intermediate- and short-range defects.

The remainder of the paper is organized as follows: the next two sections address the experimental procedures, and the computing methods and model systems, respectively. Results are presented and discussed in detail, taking into account the different experimental techniques (subsections 1–4), and the theoretical analysis based on the band structure and density of states is given (subsection 5). Finally, we summarize our main conclusions.

Experimental Procedures

Experimental details were as follows: In 80 mL of NaOH 1 M solution was added 2.6 mmol of zinc acetate. After 15 min stirring, 4.5 mL of polyethyleneglycol PEG (M_w 400) was added into the solution under constant stirring. The solution was transferred into a sealed Teflon autoclave and annealed at 130 °C for 15 min, 30 min, 1 h and 2 h using the conventional hydrothermal and the microwave-hydrothermal processing. The pressure in the sealed autoclave was stabilized at 2.0 atm. The autoclave was cooled to room temperature naturally. The ZnO precipitate was washed with water, and dried at 60 °C for 5 h.

The ZnO powders were analyzed by X-ray diffraction (XRD), using a Rigaku DMAX 2500 PC diffractometer in a $\theta-2\theta$ configuration ranging from 5° to 75°, $\lambda = 1.5406$ Å, with a graphite monochromator.

Raman data were recorded on a RFS/100/S Bruker FT-Raman spectrometer with Nd:YAG laser providing an excitation light at 1064.0 nm. The spectral resolution was 4 cm^{-1}, and 10−700 cm^{-1} spectral ranges were analyzed.

The size and morphology of ZnO particles were measured by scanning electron microcopy (SEM) and transmission electron microscopy (TEM) using a Zeiss DSM 940A model and a Philips CM 200 model, respectively. Structural formation for the particles was measured by selected-area electron diffraction (SAED).

The photoluminescence spectra were measured using a U1000 Jobin-Yvon double monochromator coupled to a cooled GaAs photomultiplier and a conventional photon counting system. The 488.0 nm exciting wavelength of an argon-ion laser was used, with the laser maximum output power kept within 25 mW. The measurements were performed using constant mass samples.

Computing Methods and Model Systems

The literature contains several studies on PL of materials disordered at room temperature with the finality to understand the why of the behavior electronic levels for gap variation.[74–76] The periodic DFT calculations with the B3LYP[77,78] hybrid functional were performed using the CRYSTAL03[79] computer code. The B3LYP functional is known to simulate the energetic, geometric, and electronic properties of materials with significantly greater accuracy.[80] This functional has been successfully employed for studies of the electronic and structural properties of diverse compounds.[81–83] The atomic centers have been described by a modified all electron basis set[84] 6-31G* for Zn and O atoms.

Two simple models were selected to simulate the effects of a slight structural deformation on the electronic structure without completely suppressing the geometry of the cell as it is depicted

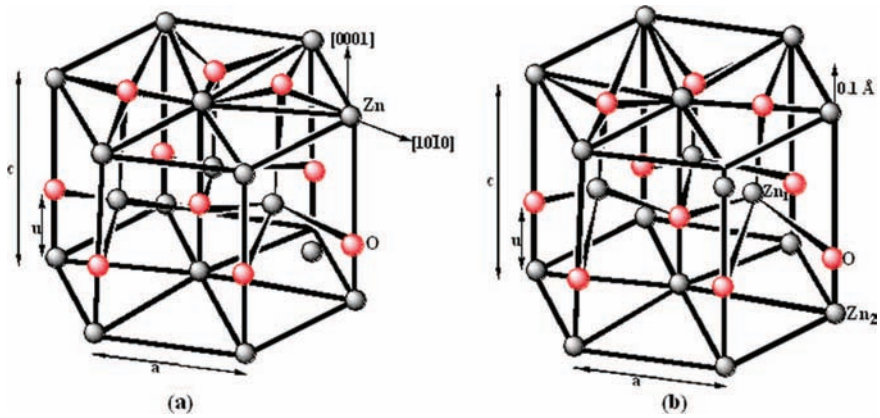

Figure 1. Primitive unit cell of the structural models of ZnO (a) ZnO-o and (b) ZnO-d.

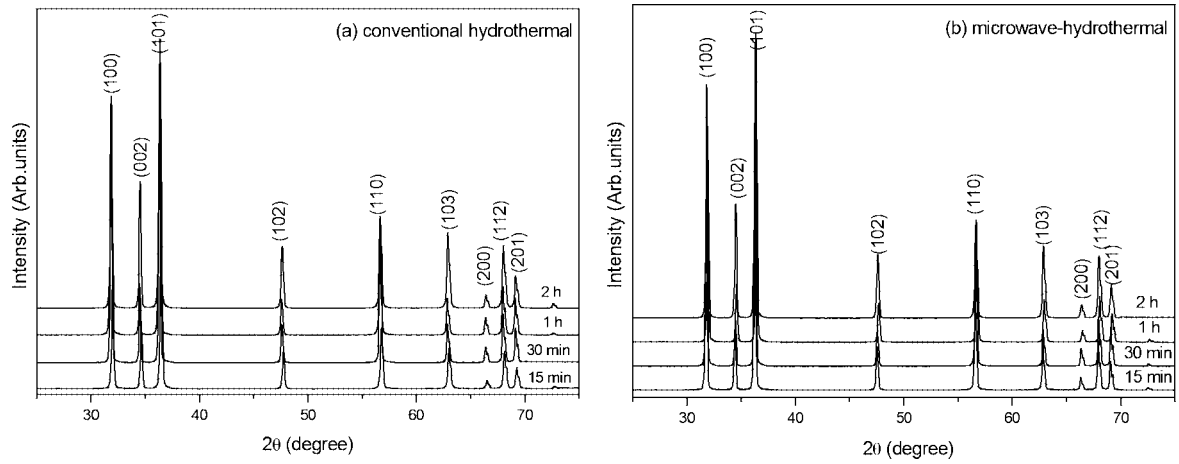

Figure 2. XRD patterns of ZnO powders obtained for 15 min, 30 min, 1 and 2 h by (a) conventional hydrothermal and (b) microwave-hydrothermal methods.

in Figure 1: the ordered ZnO-o structure and the disordered structure, named ZnO-d, in which the network of the lattice is dislocated by moving the Zn atom 0.1 Å.

These models can be useful to represent different degrees of order−disorder in the material, as well as structural defects resulting from network former displacements.

The band structures were obtained for 80 K points along the appropriate hight-symmetry paths of the adequate Brillouin zone. Diagrams of the density of states (DOS) were calculated for analysis of the corresponding electronic structure. The XcrysDen program[85] has been used for the design of band structure and DOS diagram.

Results and Discussion

1. X-ray Diffraction. A well-crystallized hexagonal wurtzite structure of ZnO was pronounced in all investigated samples (space group: $P6_3mc$ (186); $a = 3.250$ Å, $c = 5.207$ Å), according to JCPDS card 36-1451. The intensity of the relative peaks indicates the high purity of the ZnO hexagonal phase of the samples and good crystallinity, demonstrating that ZnO powders obtained by hydrothermal conditions present a long-range order or periodicity (completely ordered structure); see Figure 2a,b. No characteristics peaks for impurities were observed.

2. Raman Spectra. Figure 3a,b shows the room temperature Raman spectra of the ZnO microstructures ranging from 200 to 1200 cm^{-1}. ZnO is wurtzite structure that belongs to the space group C_{6v}^4. A_1 and E_1 are polar modes and are both Raman and infrared active, whereas the E_2 modes are nonpolar and Raman active only.[86] Both A_1 and E_1 split into transverse (TO) and longitudinal optical (LO) phonons.

The Raman spectra of ZnO powders display a narrow strong band at 435 cm^{-1} that has been assigned to one of the two E_2 modes, involving mainly Zn motion, which corresponds to band characteristic of wurtzite phase. Several common low-frequency features including bands at approximately 330 cm^{-1} should be assigned to the second order Raman spectrum arising from zone-boundary phonons $3E_{2H}-E_{2L}$, 380 cm^{-1} (A_{1T}), and the envelope of bands above 1095 cm^{-1} attributed to overtones and/or combination bands.[87,88] For the asymmetric wide band, the A_{1T} mode indicates the presence of some structural order−disorder degree in the ZnO lattice[89] that can refer to short and intermediate ranges. The samples treated for 2 h by conventional hydrothermal and microwave-hydrothermal methods present a narrower line width referring to this Raman mode (see inset of Figure 3), demonstrating the lowest short- and intermediate-range structural disorder degree in relation to other samples. However, the samples annealed at 15 min depict a broad band, indicating the higher intermediate- and short-range structural disorder. The higher ordered and higher defect densities structures are unfavorable conditions for intense photoluminescence emission.[90]

A band at 537 cm^{-1}, apparently very weak, is the contribution of the E_1 (LO) mode of ZnO associated with oxygen deficiency.[91] Regarded as an "anomalous" mode,[92] it has been variously identified as either from a second-order peak or from oxygen vacancies.[93–96] Its intensity has been observed to depend on crystallinity, crystal orientation, and on the synthesis method.

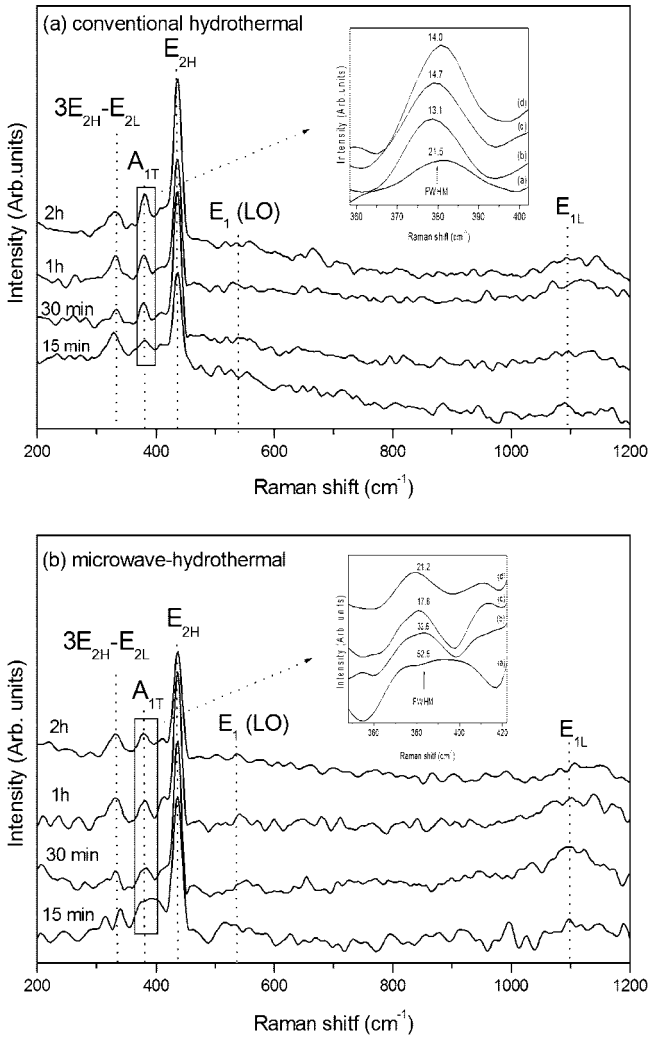

Figure 3. Raman spectra of ZnO microcrystals prepared 15 min, 30 min, 1 h and 2 h by (a) conventional hydrothermal and (b) microwave-hydrothermal methods.

The strongest E_2 mode and lowest E_1 (LO) mode indicate that a lower oxygen vacancy density is present in the samples.[97] Therefore, all ZnO samples obtained by hydrothermal conditions with and without microwave exhibited low oxygen vacancy density.

The different type of defects, such as short- and intermediate-range structural disorder, vacancies and angle distortion in the lattice, can be assigned to the interconversion of possible configurations of the wurtzite conformation during growth conditions. In the ZnO wurtzite phase the Zn_3O_3 hexagonal rings are arranged in the "boat" and "chair" configurations,[98] as presented in the Figure 4.

3. SEM and TEM. In the rapid growth of particles during the conventional hydrothermal and microwave-hydrothermal synthesis methods different configurations can be formed generating Zn and O vacancies defects and of surface, which can be responsible by different average size distributions of particles; see Figure 5.

The average particle diameters were 100 nm for the samples treated at 15 min and 1 h using the microwave-hydrothermal method, and 90 and 150 nm for the samples synthesized after 15 min and 1 h by the conventional hydrothermal method, respectively. In general, the size of the ZnO wires is uniform; however, the sample treated at 15 min by the microwave-hydrothermal method is more homogeneous with a constant

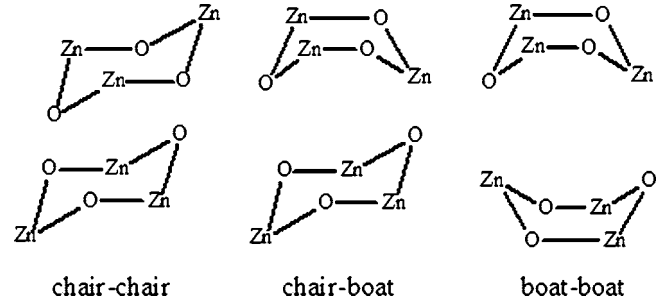

Figure 4. ZnO wurtzite-phase configurations.

diameter in the wire length. The sample obtained after 1 h under conventional hydrothermal conditions presented a bigger diameter (150 nm) and an ideal defect density that favors an intense photoluminescence, according to the PL results.

The obtained ZnO samples represent hexagonally shaped wires of high quality, as demonstrated by the SEM images illustrated in Figure 5 (inset). The SEM images reveal that the ZnO morphology is flower-like wire clusters. The clusters are composed of multiple ZnO wires joined together at one end (seed) to form the center and each grown wire is like a flower spread outward.

An individual ZnO wire for the samples obtained at 1 h under conventional hydrothermal and microwave-hydrothermal conditions is observed in the TEM images shown in Figure 6a,b. The images show sword-like ZnO wires with 300−400 nm diameter size. The SAED patterns inserted in Figure 6 show the ZnO single crystalline wire and can be indexed as the hexagonal ZnO phase. This result corroborates the XRD patterns presented in Figure 2a,b. The growth direction of the ZnO wires [001] are indicated by SAED pattern images.

A contrast thickness between center (darker) and edge (clearer), which are observed for the hexagonal transversal section structure, is shown by TEM images in Figure 6a,b. Flanges are also observed in the ZnO wire length for the sample prepared for 1 h using conventional hydrothermal methods.

An analysis of Figure 6 seems to indicate that the ZnO nanowires are faceted. The facets forming these nanowires can be polar (0001) and nonpolar $(10\bar{1}0)$ and $(11\bar{2}0)$. In this respect, in a recent theoretical analysis by our group,[84] the corresponding values of the surface energy of both polar and nonpolar facets of the ZnO system have been calculated.

4. Photoluminescence. Figure 7a,b shows the PL spectra of the ZnO powders obtained under hydrothermal conditions with and without microwaves. Numerous papers have discussed the PL behavior of crystalline ZnO. When excited by short wavelength ultraviolet radiations at room temperature, they present a predominantly blue emission band. Herein, using 488 nm excitation wavelength there is predominance of the green emission band.

Results of the PL emission of ZnO crystalline structures recorded with a 488 nm wavelength argon-ion laser indicated broad luminescence behavior in the visible-range spectra (Figure 7). In the case of samples annealed at 2 h, presenting high crystallinity (long-range order), according to XRD and Raman the PL intensity dropped to virtually zero. These well-ordered ZnO powders obtained after 2 h under hydrothermal conditions with and without microwave exhibited low emission of the red PL component and blue PL component (498 nm, blue). The powder annealed at 15 min using the conventional hydrothermal method also presented a low blue PL emission.

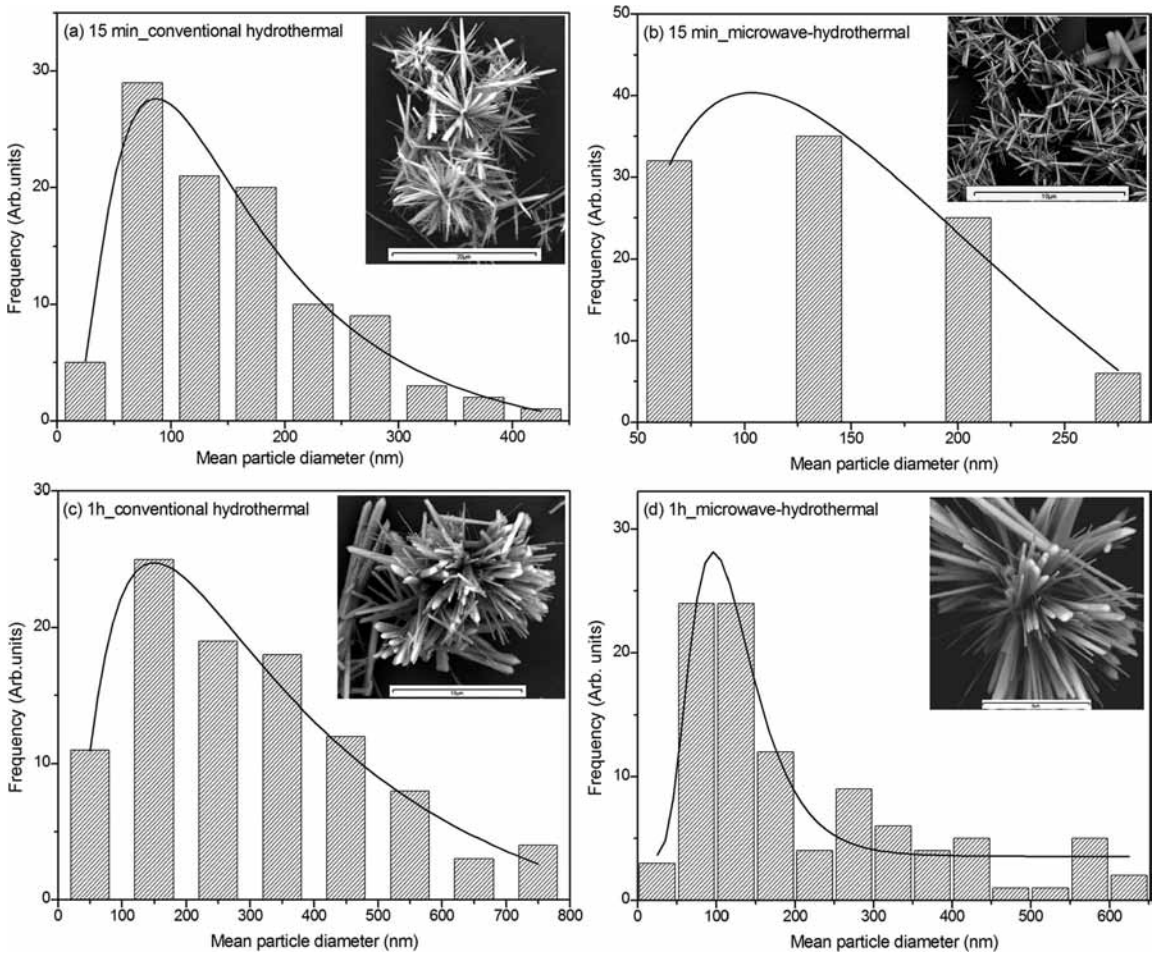

Figure 5. Mean particle diameter distribution with SEM micrographies inset: (a) 15 min using the conventional hydrothermal method; (b) 15 min using the microwave-hydrothermal method; (c) 1 h using the conventional hydrothermal method; (d) 1 h using the microwave-hydrothermal method.

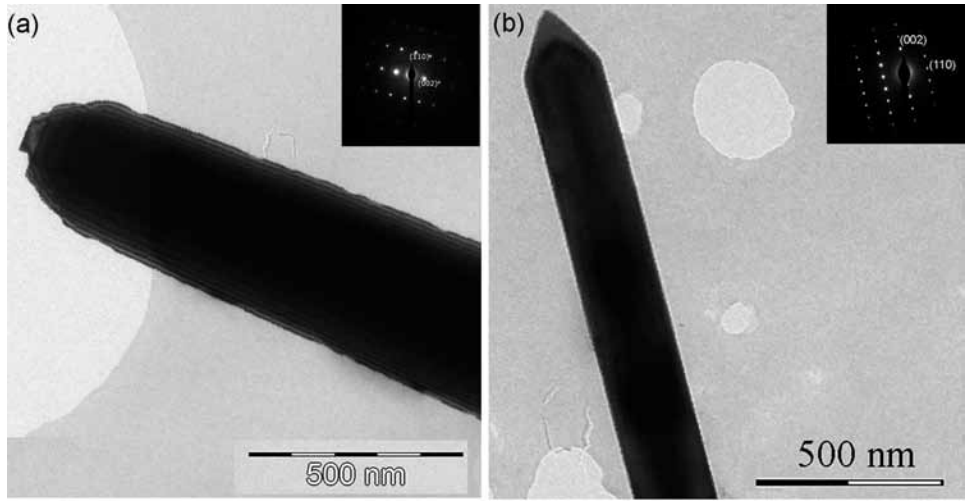

Figure 6. TEM images of ZnO crystals: (a) 1 h using the conventional hydrothermal method; (b) 1 h using the microwave-hydrothermal method. The insets are SAED patterns taken from the individual ZnO wire.

The PL curves were analyzed using a decomposition procedure with a Gaussian response function and a Fourier decomposition/filtering algorithm. The Gaussian line shape was used successfully to fit the PL peaks (inset, Figure 7). The PL curves for the all samples are composed of five or six PL components, herein two bands named green component (maximum in 532.1 and 569.2 nm), a yellow-orange component (maximum in 610.2 nm), and two red components (maximum in 653.7 and 712.6 nm). Each color represents a different type of electron transition and is linked to a specific structural arrangement.

The intensity of the green PL component increases after annealing for 15 min in both synthesis studied methods, as shown in Figure 8a,b. In this annealing time, the materials

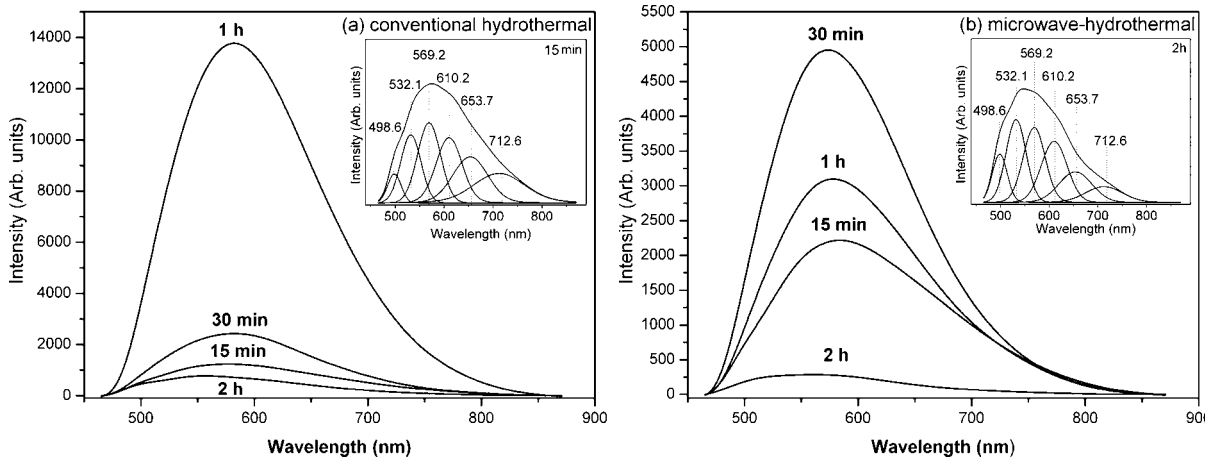

Figure 7. Photoluminescence spectra of the ZnO powders excited with the 488 nm line of an argon ion laser using (a) conventional hydrothermal and (b) microwave-hydrothermal methods. The inset is a PL decomposition curve in six Gaussian peaks.

exhibited higher structural disorder. A green maximum percentage area was observed for the sample obtained at 1 h by the conventional hydrothermal method; see Figure 8a. This high PL intensity seems to indicate that this material presents an optimum structural order−disorder degree to occur with the photoluminescence, which can be associated with different ZnO configurations during the growth step, according to Raman and particles average distribution results.

Then, disorder is linked to a modulation of oxygen in relation to the $[ZnO_4]$ cluster giving rise to interaction between the $[ZnO_3]$ clusters and V_O^x, $V_O^{\bullet}$, $V_O^{\bullet\bullet}$ species creating complex clusters. In this sense, oxygen vacancies in ZnO can occur in three different charge states: the $[ZnO_3.V_O^x]$ complex states, which present two paired electrons $\uparrow\downarrow$ and is neutral relative to the lattice, the singly ionized $[ZnO_3.V_O^{\bullet}]$ complex state, which has one unpaired electron $\uparrow$, and the $[ZnO_3.V_O^{\bullet\bullet}]$ complex state, which does not present unpaired electron and is doubly positively charged with respect to the lattice.

We speculate that these oxygen vacancies induce new energies in the band gap, which can be attributed to zinc−oxygen vacancy centers. A hole in the acceptor and an electron in a donor are created before donor excitation.

The following equations suggest that the trapped electron of oxygen vacancy in the valence band is a necessary condition for the transition of a valence-band hole in the conduction band and can be applied for disordered ZnO (intermediate and short ranges).

$$[ZnO_4]^x + [ZnO_3 \cdot V_O^x] \rightarrow [ZnO_4]' + [ZnO_3 \cdot V_O^{\bullet}] \quad (1)$$

$$[ZnO_4]^x + [ZnO_3 \cdot V_O^{\bullet}] \rightarrow [ZnO_4]' + [ZnO_3 \cdot V_O^{\bullet\bullet}] \quad (2)$$

5. Theoretical Study of the Band Structure and DOS. Over the past decade, improvements on the computational methods and the increase of computer power have made it possible to address, from first-principles calculations, condensed system problems that are difficult to address experimentally. In this section, an ordered and a disordered powder were theoretically modulated. The ordered powder can be linked to the ZnO-o theoretical model and $[ZnO_4]$ cluster. In the same way, the ZnO-d model can be linked to a structural disorder of the powder and $[ZnO_3 \cdot V_O^z]$ complex cluster where $V_O^z = V_O^x, V_O^{\bullet}, V_O^{\bullet\bullet}$. It has to be pointed out that this disorder was experimentally measured by Raman spectroscopy, TEM images and suggested thought the previous knowledge of different configurations for the ZnO.

With these models the effects of the structural disorder can be separately evaluated in terms of electronic structure. Then, a theoretical study of the band structure and density of states (DOS) projected in ordered and asymmetric models was performed.

Figure 9a reports the calculated band structure of ZnO-o. The top of the valence band (VB) and the bottom of the conduction band (CB) are both at the Γ point, indicating the gap is direct. The minimal direct gap is 2.97 eV. Figure 9b reports the calculated band structure of ZnO-d. The gap is direct in Γ point and has a value of 2.93 eV. These results indicated that structural defects induce the formation of new levels in the band gap of disorder structure. These levels are responsible for the wide PL emission.

The calculated total and atom-resolved density of states (DOS) projected for the models ZnO-o, ZnO-d are shown in Figure 9, ranging from −5 eV below the top of the VB to +11 eV above and presenting the principal orbital that influences the gap state.

For the ZnO-o, Figure 9a, the valence bands derive from $2p_x$, $2p_y$, $2p_z$ orbitals of O atoms and from transition-metal zinc ($3d_{xy}$, $3d_{xz}$, $3d_{yz}$) atomic orbitals, designated as "t_{2g}" by comparison with the $[ZnO_4]$ regular cluster. Above these six bands are four Zn ($d_{x^2}-y^2$ and $3d_{z^2}$) character bands designated as "e_g". For the displaced model ZnO-d, Figure 9b, the VB is globally constituted of O ($2p_x$, $2p_y$, $2p_z$) character states and mainly on the 3d state of zinc that was not displaced in an apparently random splitting of bands. The presence of the 3d states in the VB in the two models revel a strong bonding character between O and Zn.

The excitation line of 488 nm has a corresponding energy of 2.54 eV and are less energetic than the calculated band gap of ZnO-o and ZnO-d. Previous theoretical results have demonstrated that an increased displacement of the former lattice induces a decrease of band gap energy.[99] Then the blue and greenish luminescence are linked to shallow defects, and yellow-orange-red light, to deeply inserted levels in the band gap. With increased structural disorder there is the predominance of $V_O^{\bullet\bullet}$ species and then yellow-orange-red light emission. In the same way the $V_O^{\bullet}$ species can be linked to shallow defects and blue-green light in accordance with previous reported results.[67] Moreover, oxygen vacancies tend to trap photogenerated electrons. The charge transfer that occurs as proposed in eqs 1 and 2 creates electron and hole polarons that can be designated as bipolarons.

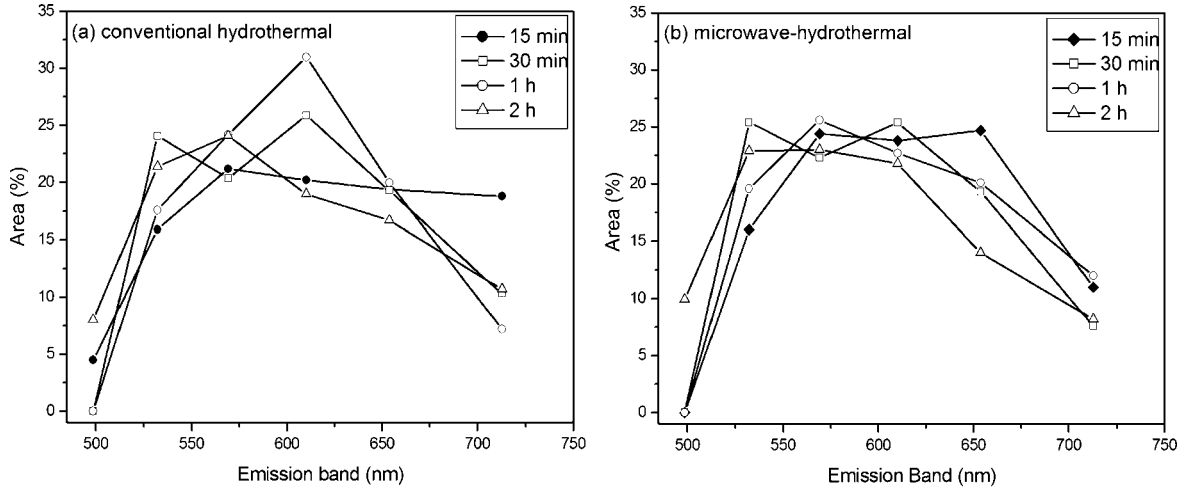

Figure 8. Graphic of emission band showing the color component percent area obtained by PL decomposition curves.

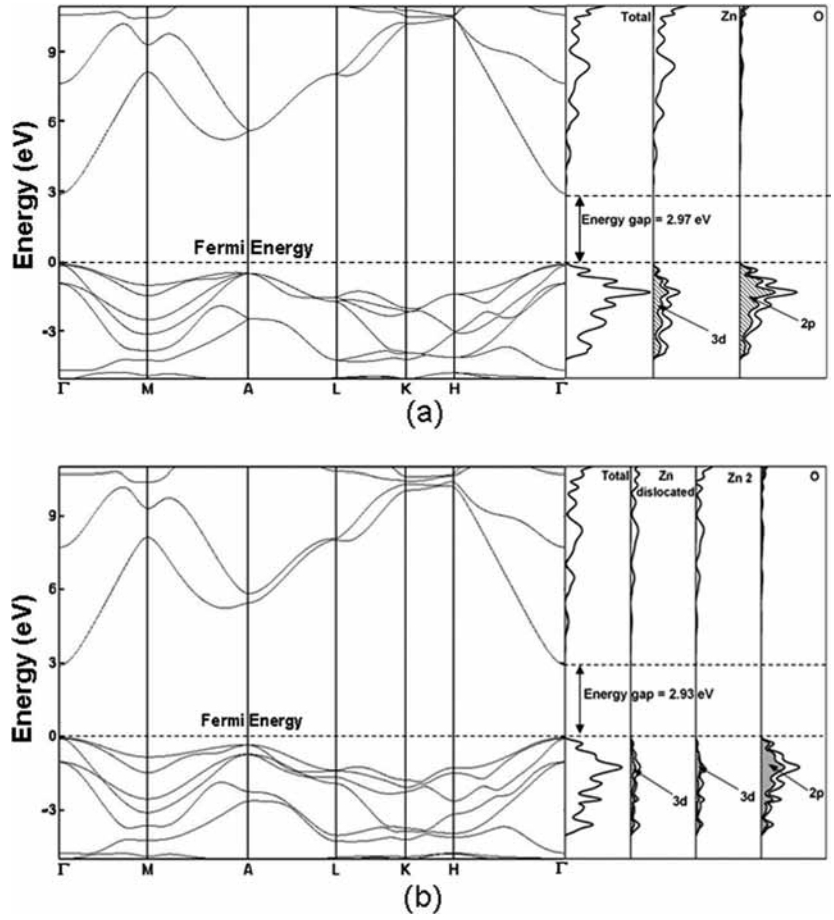

Figure 9. Calculated energy band structure and total and atom-projected density of states (DOS) for (a) ZnO-o and (b) ZnO-d.

In the complex, the $[ZnO_4]''$ clusters act as electron donors, and the vacancy complex] tends to trap electrons and/or holes and $[ZnO_3 \cdot V_O^{\bullet\bullet}]$ act as electron traps. After excitation of the photon, the recombination and decay process follows the several valid hypotheses presented in the literature.[99–102]

This disorder is produced by clusters of different coordinations $[ZnO_4]$ and $[ZnO_3 \cdot V_O^Z]$, forming nano/microentities whose size and order are determined by their time dependence. As the time increases, the stabilization forces associated with the polarization of the clusters are displaced becoming stronger than the short-range repulsive cluster−cluster interactions stabilizing the intermediate phase.

Conclusions

In summary, ZnO single crystals were easily prepared using conventional hydrothermal and microwave-hydrothermal methods and their crystalline and optical properties were carefully investigated. PL emission intensity depends on different types of defects generated by possible configuration arrangement interconversion in solution during the ZnO growth. On the basis of X-ray diffraction, Raman spectroscopy, scanning electron microscopy, transmission electron microscopy and photoluminescence analysis, it was shown that intermediate- and short-range structural order−disorder defects can be generated using

distinct synthesis methods. The theoretical results point out that these defects generate localized electronic levels above the valence band and they are associated with a symmetry breaking process, i.e., to the Zn displacement in the wurtzite ZnO type-structure.

Acknowledgment. We acknowledge the financial support of the Brazilian research financing institutions: CAPES, CNPq, and FAPESP/CEPID 98/14324-0.

References and Notes

(1) Chen, Y. F.; Bagnall, D. M.; Koh, H. J.; Park, K. T.; Hiraga, K.; Zhu, Z. Q.; Yao, T. *J. Appl. Phys.* **1998**, *84*, 3912.
(2) Huang, Y.; Duan, X. F.; Wei, Q. Q.; Lieber, C. M. *Science* **2001**, *291*, 630.
(3) Zhao, Q. X.; Willander, M.; Morjan, R. E.; Hu, Q. H.; Campbell, E. E. B. *Appl. Phys. Lett.* **2003**, *83*, 165.
(4) Gao, P. X.; Ding, Y.; Mai, W. J.; Hughes, W. L.; Lao, C. S.; Wang, Z. L. *Science* **2005**, *309*, 1700.
(5) Goldberger, J.; He, R. R.; Zhang, Y. F.; Lee, S. W.; Yan, H. Q.; Choi, H. J.; Yang, P. D. *Nature* **2003**, *422*, 599.
(6) Kawano, T.; Imai, H. *Cryst. Growth Des.* **2006**, *6*, 1054.
(7) Zhao, J.; Jin, Z. G.; Li, T.; Liu, X. X. *Appl. Surf. Sci.* **2006**, *252*, 8287.
(8) Sun, G. B.; Cao, M. H.; Wang, Y. H.; Hu, C. W.; Liu, Y. C.; Ren, L.; Pu, Z. F. *Mater. Lett.* **2006**, *60*, 2777.
(9) Xing, Y. J.; Xi, Z. H.; Zhang, X. D.; Song, J. H.; Wang, R. M.; Xu, J.; Xue, Z. Q.; Yu, D. P. *Solid State Commun.* **2004**, *129*, 671.
(10) Liu, J. P.; Huang, X. T.; Li, Y. Y.; Sulieman, K. M.; Sun, F. L.; He, X. *Scr. Mater.* **2006**, *55*, 795.
(11) Chen, Z. G.; Ni, A.; Li, F.; Cong, H. T.; Cheng, H. M.; Lu, G. Q. *Chem. Phys. Lett.* **2007**, *434*, 301.
(12) Ghoshal, T.; Kar, S.; Chaudhuri, S. *Cryst. Growth Des.* **2007**, *7*, 136.
(13) Bardhan, R.; Wang, H.; Tam, F.; Halas, N. J. *Langmuir* **2007**, *23*, 5843.
(14) Xu, F.; Yuan, Z. Y.; Du, G. H.; Halasa, M.; Su, B. L. *Appl. Phys. A: Mater. Sci. Process.* **2007**, *86*, 181.
(15) Jang, E. S.; Won, J. H.; Hwang, S. J.; Choy, J. H. *Adv. Mater.* **2006**, *18*, 3309.
(16) Illy, B.; Shollock, B. A.; MacManus-Driscoll, J. L.; Ryan, M. P. *Nanotechnology* **2005**, *16*, 320.
(17) Gao, P.; Ying, C.; Wang, S. Q.; Ye, L. N.; Guo, Q. X.; Xie, Y. *J. Nanoparticle Res.* **2006**, *8*, 131.
(18) Niu, H. X.; Yang, Q.; Tang, K. B.; Xie, Y.; Yu, F. *J. Mater. Sci.* **2006**, *41*, 5784.
(19) Xu, C. X.; Sun, X. W.; Dong, Z. L.; Yu, M. B. *Appl. Phys. Lett.* **2004**, *85*, 3878.
(20) Vayssieres, L. *Adv. Mater.* **2003**, *15*, 464.
(21) Wang, L.; Zhang, X.; Zhao, S.; Zhou, G.; Zhou, Y.; Qi, J. *Appl. Phys. Lett.* **2005**, *86*, 024108.
(22) Gao, P. X.; Wang, Z. L. *J. Phys. Chem. B* **2004**, *108*, 7534.
(23) Gao, P. X.; Wang, Z. L. *J. Appl. Phys.* **2005**, *97*, 044304.
(24) Hughes, W. L.; Wang, Z. L. *J. Am. Chem. Soc.* **2004**, *126*, 6703.
(25) Yu, H. D.; Zhang, Z. P.; Han, M. Y.; Hao, X. T.; Zhu, F. R. *J. Am. Chem. Soc.* **2005**, *127*, 2378.
(26) Suh, H. W.; Kim, G. Y.; Jung, Y. S.; Choi, W. K.; Byun, D. *J. Appl. Phys.* **2005**, *97*, 044305.
(27) Pan, Z. W.; Dai, Z. R.; Wang, Z. L. *Science* **2001**, *291*, 1947.
(28) Kong, X. Y.; Wang, Z. L. *Nano Lett.* **2003**, *3*, 1625.
(29) Kong, X. Y.; Ding, Y.; Yang, R.; Wang, Z. L. *Science* **2004**, *303*, 1348.
(30) Umar, A.; Kim, S. H.; Kim, J. H.; Park, Y. K.; Hahn, Y. B. *Mater. Lett.* **2007**, *61*, 4954.
(31) Hu, J. Q.; Li, Q.; Meng, X. M.; Lee, C. S.; Lee, S. T. *Chem. Mater.* **2003**, *15*, 305.
(32) Kong, X. H.; Sun, X. M.; Li, X. L.; Li, Y. D. *Mater. Chem. Phys.* **2003**, *82*, 997.
(33) Kong, Y. C.; Yu, D. P.; Zhang, B.; Fang, W.; Feng, S. Q. *Appl. Phys. Lett.* **2001**, *78*, 407.
(34) Chen, S. J.; Liu, Y. C.; Ma, J. G.; Zhao, D. X.; Zhi, Z. Z.; Lu, Y. M.; Zhang, J. Y.; Shen, D. Z.; Fan, X. W. *J. Cryst. Growth* **2002**, *240*, 467.
(35) Huang, M. H.; Wu, Y. Y.; Feick, H.; Tran, N.; Weber, E.; Yang, P. D. *Adv. Mater.* **2001**, *13*, 113.
(36) Gao, P. X.; Ding, Y.; Wang, I. L. *Nano Lett.* **2003**, *3*, 1315.
(37) Mensah, S. L.; Kayastha, V. K.; Ivanov, I. N.; Geohegan, D. B.; Yap, Y. K. *Appl. Phys. Lett.* **2007**, *90*, 113108.
(38) Park, W. I.; Kim, D. H.; Jung, S. W.; Yi, G. C. *Appl. Phys. Lett.* **2002**, *80*, 4232.
(39) Zhang, X. H.; Xie, S. Y.; Jiang, Z. Y.; Zhang, X.; Tian, Z. Q.; Xie, Z. X.; Huang, R. B.; Zheng, L. S. *J. Phys. Chem. B* **2003**, *107*, 10114.
(40) Wu, J. J.; Liu, S. C.; Wu, C. T.; Chen, K. H.; Chen, L. C. *Appl. Phys. Lett.* **2002**, *81*, 1312.
(41) Govender, K.; Boyle, D. S.; Kenway, P. B.; O'Brien, P. *J. Mater. Chem.* **2004**, *14*, 2575.
(42) Zhang, R.; Kerr, L. L. *J. Solid State Chem.* **2007**, *180*, 988.
(43) Fu, Z. P.; Wang, Z.; Yang, B. F.; Yang, Y. L.; Yan, H. W.; Xia, L. S. *Mater. Lett.* **2007**, *61*, 4832.
(44) Du, N.; Zhang, H.; Yang, Z. Q.; Zhai, C. X.; Yu, J. X.; Wu, J. B.; Zhang, X. B.; Yang, D. R. *Mater. Res. Bull.* **2007**, *42*, 1316.
(45) Li, Z. K.; Huang, X. T.; Liu, J. P.; Li, Y. Y.; Ji, X. X.; Li, G. G. *Mater. Lett.* **2007**, *61*, 4362.
(46) Viswanatha, R.; Santra, P. K.; Dasgupta, C.; Sarma, D. D. *Phys. Rev. Lett.* **2007**, *98*, 255501.
(47) Mo, M.; Yu, J. C.; Zhang, L. Z.; Li, S. K. A. *Adv. Mater.* **2005**, *17*, 756.
(48) Wei, A.; Sun, X. W.; Xu, C. X.; Dong, Z. L.; Yang, Y.; Tan, S. T.; Huang, W. *Nanotechnology* **2006**, *17*, 1740.
(49) Lu, C. H.; Yeh, C. H. *Ceram. Int.* **2000**, *26*, 351.
(50) Chen, D. R.; Jiao, X. L.; Cheng, G. *Solid State Commun.* **1999**, *113*, 363.
(51) Guo, L.; Ji, Y. L.; Xu, H. B.; Simon, P.; Wu, Z. Y. *J. Am. Chem. Soc.* **2002**, *124*, 14864.
(52) Ohshima, E.; Ogino, H.; Niikura, I.; Maeda, K.; Sato, M.; Ito, M.; Fukuda, T. *J. Cryst. Growth* **2004**, *260*, 166.
(53) Yoneta, M.; Yoshino, K.; Ohishi, M.; Saito, H. *Physica B* **2006**, *376*, 745.
(54) Trindade, T.; Dejesus, J. D. P.; Obrien, P. *J. Mater. Chem.* **1994**, *4*, 1611.
(55) Hu, H. M.; Huang, X. H.; Deng, C. H.; Chen, X. Y.; Qian, Y. T. *Mater. Chem. Phys.* **2007**, *106*, 58.
(56) Komarneni, S.; Roy, R.; Li, Q. H. *Mater. Res. Bull.* **1992**, *27*, 1393.
(57) Komarneni, S.; Bruno, M.; Mariani, E. *Mater. Res. Bull.* **2000**, *35*, 1843.
(58) Freeman, C. L.; Claeyssens, F.; Allan, N. L.; Harding, J. H. *Phys. Rev. Lett.* **2006**, *96*, 066102.
(59) Botello-Mendez, A. R.; Martinez-Martinez, M. T.; Lopez-Urias, F.; Terrones, M.; Terrones, H. *Chem. Phys. Lett.* **2007**, *448*, 258.
(60) De la Rosa, E.; Sepulveda-Guzman, S.; Reeja-Jayan, B.; Torres, A.; Salas, P.; Elizondo, N.; Yacaman, M. J. *J. Phys. Chem. C* **2007**, *111*, 8489.
(61) Vanheusden, K.; Seager, C. H.; Warren, W. L.; Tallant, D. R.; Voigt, J. A. *Appl. Phys. Lett.* **1996**, *68*, 403.
(62) Van Dijken, A.; Meulenkamp, E. A.; Vanmaekelbergh, D.; Meijerink, A. *J. Phys. Chem. B* **2000**, *104*, 1715.
(63) Vanheusden, K.; Warren, W. L.; Seager, C. H.; Tallant, D. R.; Voigt, J. A.; Gnade, B. E. *J. Appl. Phys.* **1996**, *79*, 7983.
(64) Hsu, J. W. P.; Tallant, D. R.; Simpson, R. L.; Missert, N. A.; Copeland, R. G. *Appl. Phys. Lett.* **2006**, *88*, 252103.
(65) Djurisic, A. B.; Leung, Y. H.; Tam, K. H.; Hsu, Y. F.; Ding, L.; Ge, W. K.; Zhong, Y. C.; Wong, K. S.; Chan, W. K.; Tam, H. L.; Cheah, K. W.; Kwok, W. M.; Phillips, D. L. *Nanotechnology* **2007**, *18*, 095702.
(66) Dingle, R. *Phys. Rev. Lett.* **1969**, *23*, 579.
(67) Wang, J. M.; Gao, L. *Solid State Commun.* **2004**, *132*, 269.
(68) Lin, B.; Fu, Z.; Jia, Y. B. *Appl. Phys. Lett.* **2001**, *79*, 943.
(69) Reynolds, D. C.; Look, D. C.; Jogai, B.; Morkoc, H. *Solid State Commun.* **1997**, *101*, 643.
(70) Zhang, S. B.; Wei, S. H.; Zunger, A. *Phys. Rev. B* **2001**, *63*, 75205.
(71) Anpo, M.; Kubokawa, Y. *J. Phys. Chem.* **1984**, *88*, 5556.
(72) Schoenmakers, G. H.; Vanmaekelbergh, D.; Kelly, J. J. *J. Phys. Chem.* **1996**, *100*, 3215.
(73) Sun, Y.; Ashfold, M. N. R. *Nanotechnology* **2007**, *18*, 245701.
(74) Longo, E.; Orhan, E.; Pontes, F. M.; Pinheiro, C. D.; Leite, E. R.; Varela, J. A.; Pizani, P. S.; Boschi, T. M.; Lanciotti, F.; Beltran, A.; Andres, J. *Phys. Rev. B* **2004**, *69*, 125115.
(75) Orhan, E.; Varela, J. A.; Zenatti, A.; Gurgel, M. F. C.; Pontes, F. M.; Leite, E. R.; Longo, E.; Pizani, P. S.; Beltran, A.; Andres, J. *Phys. Rev. B* **2005**, *71*, 085113.
(76) Orhan, E.; Pontes, F. M.; Pinheiro, C. D.; Longo, E.; Pizani, P. S.; Varela, J. A.; Leite, E. R.; Boschi, T. M.; Beltran, A.; Andres, J. *J. Eur. Ceram. Soc.* **2005**, *25*, 2337.
(77) Becke, A. D. *J. Chem. Phys.* **1993**, *98*, 5648.
(78) Lee, C. T.; Yang, W. T.; Parr, R. G. *Phys. Rev. B* **1988**, *37*, 785.
(79) Saunders, V. R.; Dovesi, R.; Roetti, C.; Orlando, R.; Zicovich-Wilson, C. M.; Harrison, N. M.; Doll, K.; Civalleri, B.; Bush, I. J.; D'Arco, P. In *CRISTAL03 User's Manual*, University of Torino, Torino, Italy, 1998.
(80) Corà, F.; Alfredsson, M.; Mallia, G.; Middlemiss, D. S.; Mackrodt, W.; Dovesi, R.; Orlando, R. *Struct. Bonding (Berlin)*; Springer-Verlag: Berlin, 2004; Vol. 113.

(81) Longo, V. M.; Cavalcante, L. S.; Erlo, R.; Mastelaro, V. R.; de Figueiredo, A. T.; Sambrano, J. R.; de Lázaro, S.; Freitas, A. Z.; Gomes, L., Jr.; Varela, J. A.; Longo, E. *Acta Material.* **2007**, *12*, 05910.1016/j.actamat.

(82) Sambrano, J. R.; Longo, V. M.; Longo, E.; Taft, C. A. *J. Mol. Struct. (THEOCHEM)* **2007**, *813*, 49.

(83) de Lazaro, S.; Longo, E.; Sambrano, J. R.; Beltran, A. *Surf. Sci.* **2004**, *552*, 149.

(84) Marana, N. L.; Longo, V. M.; Longo, E.; Martins, J. B. L.; Sambrano, J. R. *J. Phys. Chem. A*, DOI 10.1021/jp801718x.

(85) Kokalj, A. *J. Mol. Graph.* **1999**, *17*, 176.

(86) Cusco, R.; Alarcon-Llado, E.; Ibanez, J.; Artus, L.; Jimenez, J.; Wang, B. G.; Callahan, M. J. *Phys. Rev. B* **2007**, *75*, 165202.

(87) Ozgur, U.; Alivov, Y. I.; Liu, C.; Teke, A.; Reshchikov, M. A.; Dogan, S.; Avrutin, V.; Cho, S. J.; Morkoc, H. *J. Appl. Phys.* **2005**, *98*, 041301.

(88) Damen, T. C.; Porto, S. P. S.; Tell, B. *Phys. Rev.* **1966**, *142*, 570.

(89) Donga, Z. W.; Zhang, C. F.; Dengc, H.; You, G. J.; Qian, S. X. *Mater. Chem. Phys.* **2006**, *99*, 160.

(90) de Figueiredo, A. T.; Longo, V. M.; de Lazaro, S.; Mastelaro, V. R.; De Vicente, F. S.; Hernandes, A. C.; Li, M. S.; Varela, J. A.; Longo, E. *J. Lumin.* **2007**, *126*, 403.

(91) Windisch, C. F.; Exarhos, G. J.; Yao, C. H.; Wang, L. Q. *J. Appl. Phys.* **2007**, *101*, 123711.

(92) Bundesmann, C.; Ashkenov, N.; Schubert, M.; Spemann, D.; Butz, T.; Kaidashev, E. M.; Lorenz, M.; Grundmann, M. *Appl. Phys. Lett.* **2003**, *83*, 1974.

(93) Wang, X.; Li, Q. Q.; Liu, Z. B.; Zhang, J.; Liu, Z. F.; Wang, R. M. *Appl. Phys. Lett.* **2004**, *84*, 4941.

(94) Wu, J. J.; Liu, S. C. *J. Phys. Chem. B* **2002**, *106*, 9546.

(95) Shi, Q. F.; Rendek, L. J.; Cai, W. B.; Scherson, D. A. *Electrochem. Solid State Lett.* **2003**, *6*, E35.

(96) Xu, J. F.; Ji, W.; Wang, X. B.; Shu, H.; Shen, Z. X.; Tang, S. H. *J. Raman Spectrosc.* **1998**, *29*, 613.

(97) Chen, S. J.; Liu, Y. C.; Lu, Y. M.; Zhang, J. Y.; Shen, D. Z.; Fan, X. W. *J. Cryst. Growth* **2006**, *289*, 55.

(98) Claeyssens, F.; Freeman, C. L.; Allan, N. L.; Sun, Y.; Ashfold, M. N. R.; Harding, J. H. *J. Mater. Chem.* **2005**, *15*, 139.

(99) Leonelli, R.; Brebner, J. L. *Solid State Commun.* **1985**, *54*, 505.

(100) Leonelli, R.; Brebner, J. L. *Phys. Rev. B* **1986**, *33*, 8649.

(101) Eglitis, R. I.; Kotomim, E. A.; Bostel, G. *Eur. Phys. J. B* **2002**, *27*, 483.

(102) Eglitis, R. I.; Kotomim, E. A.; Bostel, G. *J. Phys.: Condens. Matter* **2002**, *14*, 3735.

JP8022474